Muhammad Zakaria[1]
Abbas M. Sharaky[1]
Al-Sayed Al-Sherbini[2]
Mohamed Bassyouni[3,4,*]
Mashallah Rezakazemi[5]
Yasser Elhenawy[6]

Water Desalination Using Solar Thermal Collectors Enhanced by Nanofluids

The absorption efficiency of a solar collector using different types of nanofluids was improved. Experimental work was carried out to investigate the flat-plate and evacuated-tube collectors under outdoor conditions to produce distilled water. A pilot plant was designed and installed. The yield of distilled water at different seawater flow rates and the physical properties of nanofluids were determined. Solar intensity, water mass flow rate, and temperature were measured. The performance of the desalination unit was evaluated in the presence of carbon nanotubes in paraffin wax and ethylene glycol nanofluids. The evaporation efficiency of the flat-plate collector was improved up to 36 % in the presence of ethylene glycol nanofluid at 80–100 °C.

Keywords: Desalination, Evacuated-tube collector, Flat-plate collector, Nanofluids, Solar energy

Received: July 24, 2021; *revised:* October 12, 2021; *accepted:* October 22, 2021

DOI: 10.1002/ceat.202100339

1 Introduction

In future, the world is confronted with energy and freshwater shortage. Desalination of brackish or seawater is one of the most important ways to solve the water scarcity issue [1, 2]. The use of solar energy or waste heat sources is acceptable for water-producing systems of such a small size [3–5]. The relevancy of nanomaterials is to realize the best attainable properties within the smallest possible loadings through homogenized distribution and stable suspension of these nanoparticles [6–11]. Often, heat transfer improvement in solar collectors is one of the basic problems in energy saving, compact designs, and different operating temperatures. Researchers also investigated the multiwalled carbon nanotubes (MWCNTs) and water nanofluids with a pH of 3.5, 6.5, and 9.5, and Triton X-100 as a surfactant (0.2 wt %) using flat-plate solar collectors. It was found that the nanofluids have better heat transfer performance in acidic and alkaline water due to the influence of the isoelectric point. The higher efficiency (67 %) was obtained at pH 9.5 and 3.5 with a water flow rate of 0.0333 kg s^{-1}.

A stable nanofluid based on ethylene glycol-containing nanosheets of graphene oxide was prepared by Yu et al. [12]. The improvement in thermal conductivity relies strongly on the volume fraction of the nanosheet of graphene oxide and increases with higher nanoparticle loading. The heat efficiency was enhanced up to 61.0 % using a nanosheet loading of 5.0 vol %. For seven days, the thermal conductivity of the fluids remained almost constant, which suggests their high stability. In the measured temperature range, the enhancement value was independent of the temperature.

Peyghambarzadeh et al. [13, 14] studied force convection techniques in an excessively base water nanofluid, which was experimentally compared to water in a vehicle heat exchanger with different nanofluid loadings. It was experimentally investigated to improve the rate of heat transfer. The variable effect of the inlet temperature of the fluid in the heat exchanger on the heat transfer coefficient was evaluated. The findings showed that the incremental fluid circulation rate would increase the output rate of heat transfer, while the temperature of the fluid entering the heat exchanger had negligible effects. Meanwhile, water nanofluid subservience at low volume loadings would increase the heat transfer rate efficiency by approximately 44 % compared to water.

[1]Muhammad Zakaria, Prof. Abbas M. Sharaky
Department of Natural Resources, Institute of African Research and Studies, Cairo University, Giza, Egypt.

[2]Prof. Al-Sayed Al-Sherbini
Department of Measurements, Photochemistry and Agriculture Applications, National Institute of Laser Enhanced Science (NILES), Cairo University, Cairo, Egypt.

[3]Prof. Mohamed Bassyouni
migb2000@hotmail.com
Department of Chemical Engineering, Faculty of Engineering, Port Said University, Port Fouad, 42526, Egypt.

[4]Prof. Mohamed Bassyouni
University of Science and Technology, Materials Science Program, Zewail City of Science and Technology, October Gardens, 6th of October, Giza, 12578, Egypt.

[5]Prof. Mashallah Rezakazemi
Faculty of Chemical and Materials Engineering, Shahrood University of Technology, Shahrood, Iran.

[6]Prof. Yasser Elhenawy
Department of Mechanical Power Engineering, Faculty of Engineering, Port Said University, Port Said, 42526, Egypt.

Chandrasekar et al. [15] analyzed the performance and the rate of heat transfer by forced convection characteristics of varied nanofluids. It was found that the performance of heat transfer depends on several parameters such as dispersibility of nanoparticles, viscosity, particle shape, and velocity profile.

Hashemabadi and Etemad [16] investigated the impact of circular angle on the second-rate flow of elastic fluids through the non-circular passage. It was found that the amount of aluminum oxide nanoparticles mixed in a fluid of water can improve the rate of heat transfer of a heat exchanger for automobiles. The efficiency of heat transfer improved up to 50 % in the presence of 1 vol % aluminum oxide.

Taylor et al. [17] studied a concentrated solar thermal system based on copper, graphite, aluminum, and silver nanofluids for power electricity generation of 10–100 MW_e. They stated that different nanofluids produced modest variations in system efficiency of less than 2 % for equivalent solar absorption. Improvement in thermal efficiency was obtained in the range of 5–10 % using 0.001 vol % nanofluid.

Yousefi et al. [18] examined the impact of aluminum oxide (Al_2O_3) mixing with water to prepare a nanofluid as an operating fluid for improved flat-plate collector (FPC) efficiency. In distinction to the literature review during this set, their experimental results showed that the thermal effeciency improved by about 29 % in the presence of Al_2O_3 nanofluid at 0.2 % nanoparticle loading.

Moghadam et al. [19] studied the influence of CuO/water nanofluid (0.5 vol %) on the thermal efficiency of a solar collector. The experimental results indicated that the nanofluid raised the collector efficiency by 22 % at a flow rate of 1 L min^{-1}.

Karami et al. [20] analyzed nanofluid-containing carbon nanotubes as an absorbing liquid in daylight. In their studies, the extinction coefficient of the binary compound suspension demonstrated a major enhancement over the original liquid. It is worth to mention that adding only 150 ppm functional carbon nanotubes to an alkaline aqueous solution improved the thermal conductivity up to 30 %.

Said et al. [21] investigated the performance of an FPC in the presence of TiO_2 nanofluid. The nanoparticle loading was in the range of 0.2–0.4 % at a flow rate of 0.4–1.6 L min^{-1}. Their results pointed to a significant improvement in the thermal efficiency up to 77 % using a nanoparticle loading of 0.2 % and a flow rate of 0.4 L min^{-1}.

Lin and Al-Kayiem [22] experimentally studied the copper nanopartiles/phase change material (PCM) for storage of solar energy within a range of 0.5–2 wt %. The thermal conductivity of Cu/PCM nanocomposite materials increased from 14.0 % to 47 %.

Assael et al. [23] indicated that using 1 vol % MWCNTs enhanced the thermal conductivity of water by about 40 %. Proper combination and stabilization of the particles are necessary to organize nanofluids by dispersing nanoparticles within the base fluid. Nanoparticles in the size range of 1 to 100 nm were employed.

Yu et al. [24] used a mixture of Cu nanoparticles and ethylene glycol to provide nanofluids. The copper nanoparticles (0.33 vol %) showed a 40 % increase in the thermal conductivity of the fluids.

Such studies confirmed that the thermophysical properties of numerous fluids may be enhanced through the addition of small loadings of nanoparticles. The kinds of nanoparticles studied consist of pure metals, metal oxides, carbides, and diverse carbon materials. Many of these varieties of nanoparticles were integrated into fluids which include water and oil in ethylene glycol. Gold (Au), silver (Ag), and other nanoparticles were investigated due to their superior chemical, electrical, and optical properties in nanoscale [25–34]. Eastman et al. [35] found that copper oxide nanoparticles will give up to 65 % improvement in thermal conductivity of nanofluids for several industrial applications. Likewise, they found a rise in thermal conductivity up to 45 % for a nanofluid including a little loading of aluminum oxide nanoparticles.

Karami et al. [36] found an enhancement in thermal properties of carbon nanotubes (CNTs) compared to base water. The thermal conductivity was improved up to 30 wt % in the presence of CNTs. It was concluded that treating of CNTs with carboxylate enhanced the dispersion stability. Therefore, CNT/H_2O nanofluids become an acceptable candidate for absorption at lower temperature in solar collectors [37]. Carbon monoxide/graphene ethylene glycol (0–0.06 wt %) provided a thermal enhancement up to 6.47 % [38]. Single-walled carbon nanotubes/oil nanofluid in the range of 0.25–1 vol % led to a thermal enhancement from 10 % to 46 %, respectively [39, 40].

The thermal efficiency of a solar collector was improved up to 88 % using a carbon nanofluid at 313 K [41]. Hosseini and Dehaj [42] studied two samples of water-based TiO_2 nanofluids. The spherical and wire-like geometry (TiO_2 NPs-nanofluid, TiO_2 NWs-nanofluid) were experimentally investigated. The results showed that TiO_2 NWs-nanofluid had better thermal properties because of the specific structure of the wire-like suspended particles. The TiO_2 NWs-nanofluid and TiO_2 NPs-nanofluid increased the maximum collector efficiency up to 21.1 % and 12.2 %, respectively at 0.5 L min^{-1}.

The experimental results indicate that nanoparticles can significantly boost the photothermal conversion efficiency of solar collectors. The photothermal conversion efficiency of the bottom irradiation mode reaches ~45 % when the TiN nanoparticles loading is 0.003 wt % [43].

This article focuses on the use of nanofluids to enhance the evaporation rate in order to increase the solar thermal performance of solar collectors in water desalination. By increasing the MWCNTs loading, the evaporation rate rises. Modified paraffine and wax nanofluids are employed, having the advantage in storing latent heat in the presence of MWCNTs. The performance of two types of solar collectors, namely, flat-plate collector (FPC) and evacuated-tube collector (ETC), was evaluated in the presence of paraffine-filled MWCNTs and ethylene glycol-MWCNTs nanofluid.

2 Experimental Setup

2.1 System Description

A solar desalination unit using nanotechnology with two configurations of solar collectors was designed and implemented at the Port Said University, Egypt. The schematic outline of the

experimental setup of the FPC and evacuated tube heat pipe collector (ETC) illustrated in Fig. 1. The first configuration is equipped mainly by an FPC water collector and a seawater tank. The second configuration consists of the ETC and a seawater tank. The seawater was heated by a solar water collector and then the brine water was collected. The structure of the FPC in the presence of paraffin wax is also presented in Fig. 1. In each configuration, the solar collectors were designed and fabricated with the same dimensions.

In this work, the FPC was used as brine heater. The dimensions of the heater were 0.5 m×1 m×0.15 m. It consisted of a 0.003 m thick glass cover, insulated container, and matt black painted metal sheet. The dimensions of the absorber plate were 0.50 m×1 m×0.0007 m ($W \times L \times T$). It was placed horizontally in the center of the container. The insulation thickness under the absorber plate was 0.03 m. The container of the solar water heater collector was made of a galvanizing sheet with 0.002 m thickness. A plate of the metallic sheet absorber was coated by matt black paint. The solar water heater was placed with a tilt angle of 30°. The second heating system consisted of an evacuated tube solar collector. The specifications of the ETC are listed in Tab. 1.

Table 1. ETC specifications.

Properties	Value
Number of evacuated tubes [–]	10
Grid dimensions (length, height) [m]	0.907, 1.960
Aperture area [m^2]	1.21
Efficient solar absorption area [m^2]	1.04
Capacity of fluid in copper pipe [L]	1.0
Max working pressure [bar]	6
Insulation	Rock wool

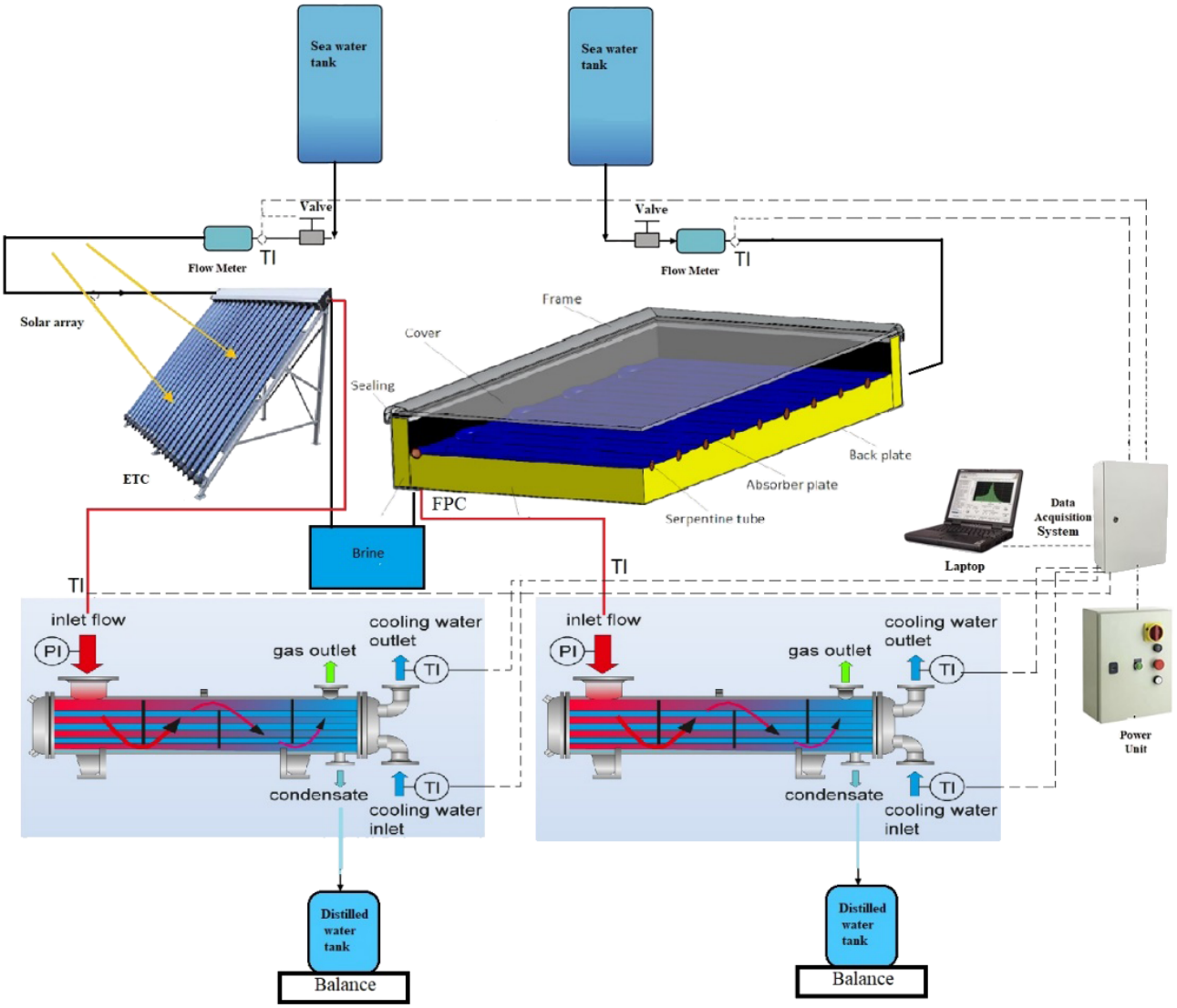

Figure 1. Schematic diagram of the experimental setup: (a) FPC, (b) ETC desalination system.

Fig. 2 displays the steps for assembling the copper tubes including paraffin wax or ethylene glycol (EG) to be placed around the heat pipes to transfer heat to the header of the ETC. The first step was removing the glass tube and heat pipe from the solar collector as indicated in Fig. 2a. The second step was the copper tube of a diameter greater than the diameter of the heat pipe as depicted in Fig. 2b. The mixture of nanomaterials was then placed between the copper tubes and the heat pipes. Then, it was installed in the header of the solar collector. In the third step, the glass tubes were installed (Fig. 2c).

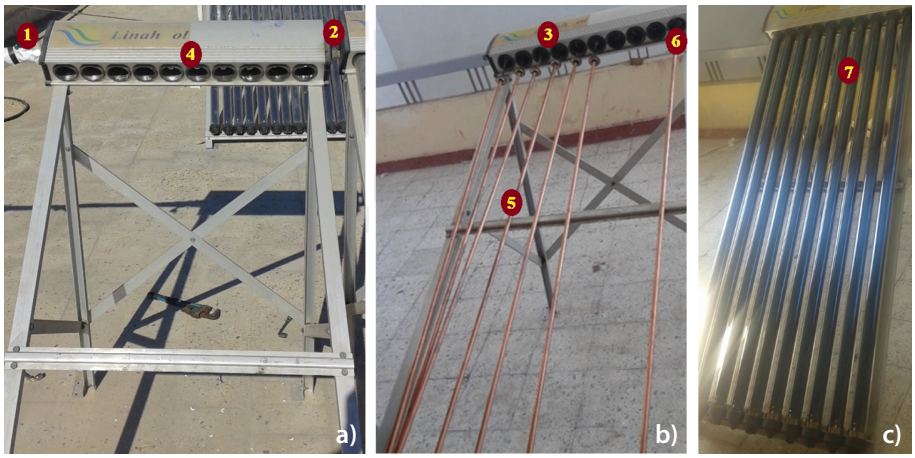

Figure 2. Evacuated-tube collector (ETC). (1) Seawater inlet (cold stream), (2) seawater outlet (hot stream), (3) copper manifold (heat exchanger), (4) holes to install glass tube, (5) hollow copper tube, (6) heat pipe condenser, (7) double-walled vacuum insulation tube.

The condenser was a shell and tube heat exchanger. The cold water flowed inside the tubes while the vapor condensed in the shell. Figs. 3a and b present the schematic diagram of the condenser. Dimensions, surface area, and selected materials for the condenser are listed in Tab. 2.

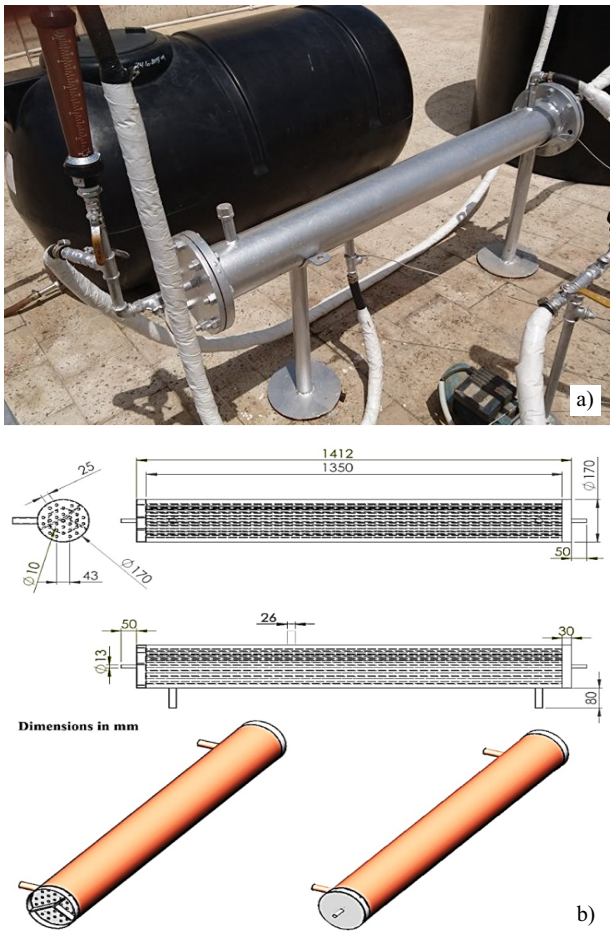

Figure 3. Layout of the condenser.

Table 2. Heat exchanger (shell and tube condenser) specifications.

Properties	Value
Shell diameter [mm]	170
Tube diameter [mm]	10
Length [mm]	1350
No. of tubes [–]	30
Material type	Copper
Thermal conductivity [$W\,m^{-1}K^{-1}$]	380
Total condenser area [m^2]	1.27

2.2 Materials and Methods

Reagent-grade chemical components were used in all experiments. Commercial MWCNTs nanoparticles with 99.99 % purity and 50 nm average diameter were deposited in the base fluid (Sigma-Aldrich GmbH). The MWCNTs-based nanofluid was selected because of high thermal conductivity, low density, and low settling rate due to Brownian motion superiority [44]. The physical properties of MWCNTs nanoparticles and the base fluid are defined in Tab. 3.

Table 3. Physical properties of MWCNTs nanoparticles, paraffin wax, and ethylene glycol.

	Density [$kg\,m^{-3}$]	Specific heat [$J\,kg^{-1}K^{-1}$]	Thermal conductivity [$W\,m^{-1}K^{-1}$]
MWCNTs [45]	2100	720	2250
Paraffin wax [46]	900	2140	0.21
Ethylene glycol [47]	1038.4	3750	0.46

The main properties of nanofluids that are used to calculate the useful thermal energy extracted during the heating phase are density ρ_{nf}[1)] and heat power C_{nf}, which may differ from those of the base fluid. Because the density and heat capacity of MWCNTs nanofluids at various nanoparticle volume loadings were not measured by the authors, the equations predicted by Xuan and Roetzel [48] were employed to calculate the density and heat capacity:

$$\rho_{nf} = (1-\phi)\rho_{bf} + \phi\rho_p \quad (1)$$

$$(\rho C)_{nf} = (1-\phi)(\rho C_p)_{bf} + \phi(\rho C_p)_p \quad (2)$$

where the subscripts f, p, and nf are assigned to base fluid, nanoparticle, and nanofluid, respectively. The thermal of conductivity K_{nf} of the nanofluid is evaluated using the Hamilton-Crosser predicted model [49] as follows:

$$K_{nf}/k_f = \frac{k_p + (n-1)k_f + (n-1)\phi(k_p - k_f)}{k_p + (n-1)k_f - \phi(k_p - k_f)/k_p} \quad (3)$$

where n is the particle shape factor identified as $n = 3/\varphi$, where φ refers to the particle sphericity. For cylindrical and spherical particles, the sphericity value is 0.5 and 1.0, respectively. Thus, in the current research, the value of n is assumed to be 6 owing to the cylindrical form of the MWCNTs nanoparticles. The calculated thermophysical properties of MWCNTs nanofluids as a function of the nanoparticles volume concentration are given in Tab. 4.

3 Measurements

The quality of distillate was measured by the total dissolved solids (TDS) contents with the temperature element model CDHSD1, Omega engineering, USA. The average TDS value of purified and seawater was 200 and 130 000 ppm, respectively, with an accuracy of ±2 % of reading below 66 000 ppm. A digital balance determined the amount of distilled water. The temperature of seawater at inlet and exit from the air solar collector was measured using Testo 825 non-contact infrared thermometers. The accuracy of the thermometers was ±1 °C of the measured value. The wind velocity was assessed using a rotating vanes anemometer manufactured by Testo Company (model Testo 435). The vane probe had a measuring wind velocity range of 0.1 up to 30 m s^{-1} with a resolution of 0.01 m s^{-1}. The total solar intensity was assessed with a pyranometer manufactured by Kipp & Zonen (model CMP 21) with an accuracy of 0.0135 W m^{-2}.

In solar desalination configurations, another factor is considered for assessing the thermal performance of the solar desalination system, explicitly the collector efficiency (η_c), that links the heat consumed to generate water evaporation to the sum of thermal energy provide outwardly.

The collector efficiency is determined by [50]:

$$\eta_c = \frac{Q_u}{A_c G} \quad (4)$$

where A_c is the solar collector area (m^2), G is the solar intensity (W m^{-2}) and Q_u is the useful heat transfer (W).

The useful heat transfer delivered was calculated as:

$$Q_u = m_f C_p (T_{co} - T_{ci}) \quad (5)$$

where mf is the feed water flow rate (kg h^{-1}), Cp is the feed water heat capacity (kWh kg^{-1}K^{-1}), Tci is the collector inlet temperature (°C), and Tco is the collector outlet temperature (°C).

The main objective of the solar desalination operation is to produce a high quantity of water evaporation with the lowest possible energy. The evaporation efficiency can be determined by Eq. (6) [51]:

$$\eta_{evp} = \frac{m_v}{m_w} \quad (6)$$

where mv is the amount of water evaporation (kg h^{-1}), and mw is the amount of seawater (kg h^{-1}).

4 Uncertainty Analysis

The uncertainties for the instruments that are used in the experimental work are determined by Eq. (7) [52, 53]:

$$u = a/\sqrt{3} \quad (7)$$

where a denotes the accuracy of the instrument and the uncertainty of standard is u (Tab. 5).

Table 4. Nanofluid thermophysical properties.

Volume concentration ϕ [vol %]	Density ρ [kg m^{-3}]	Specific heat C_{nf} [J kg^{-1}K^{-1}]	Thermal conductivity k [W m^{-1}K^{-1}]
Paraffin wax with 0.01 % MWCNTs	912	2107.3	468.22
Ethylene glycol with 0.01 % MWCNTs	1049	3688	1035

1) List of symbols at the end of the paper.

Table 5. Instrument accurateness and uncertainties of standard.

Device	Accuracy	Range	Standard uncertainty
Pyranometer	0.018 W m^{-2}	0–2400 W m^{-2}	0.01 W m^{-2}
Thermometers	1 °C	0–200 °C	0.57 °C
Salinity transducer	10 ppm	0–66 000 ppm	5.7 ppm
Velocity	0.01 m s^{-1}	0.2–40 m s^{-1}	0.0057 m s^{-1}
Balance	0.4 g	1–10 000 g	0.231 g

5 Results and Discussion

The system's performance was experimentally examined. The effect of driving parameters including temperature, feedwater flow rate, base fluid, and concentration of carbon nanotubes and type of collectors on the evaporation and desalination efficiency were justified and measured. The results were collected and plotted for the two different types of collectors (flat-plate and evacuated-tubes) and two types of base fluids (paraffin wax and ethylene glycol). The experimental data were obtained in August and September 2020. Experimental data such as the inlet feed water temperature, solar intensity, and wind speed were considered as variable parameters. Therefore, all measurements that depend on variable parameters should be determined within three excessive days to avoid margin change in solar intensity and wind speed. Two different types of nanofluid were used. Paraffin wax and ethylene glycol in the presence of 0 and 0.5 wt % of MWCNTs were utilized for both FPC and ETC. The operating time was 6 h per day.

5.1 Performance of Flat-Plate Collector and Evacuated-Tube Collector

In this system, the experiments were implemented using solar energy. Fig. 4 demonstrates the distribution of solar radiation and collector's outlet temperature at different MWCNTs loadings with paraffin wax during the day. The variations of solar intensities were acquired by the collectors with time for four consecutive days from September 04 to 07, 2020. The result indicates a variance in solar intensity with time for the run through the day with a peak solar intensity of around 900 W m^{-2}. In addition, the result illustrates the distribution of measured outlet temperature for the FPC and ETC along the day. Evaporation efficiency was determined for the nanofluid (MWCNTs, 0.5 wt %) with paraffin wax system and pure fluid using the seawater (35 000 ppm). Seawater was fed to the FPC at a flow rate of 1.35 kg h^{-1} and at 1.55 kg h^{-1} for the ETC. All temperatures showed a similar behavior as they increase with stronger solar radiation during the day.

It is also noticed from Fig. 4 that the outlet temperatures of the ETC are higher than those of the FPC, since the heat loss in the ETC is less. Because there is no insulation on the glass side of FPCs, they lose more heat to the environment than ETCs. Because tubes must be spaced apart, ETCs have a lower absorber-to-gross area ratio (usually 60–80 % less) than FPCs.

Fig. 5 demonstrates the enhancement in the evaporation efficiency through the FPC and ETC when 0.5 % MWCNTs loading is used with paraffin wax compared with pure wax. The evaporation efficiency was improved by about 27.5 % for the FPC and 13 % for the ETC at seawater flow rates of 1.35 and 1.55 kg h^{-1}, respectively.

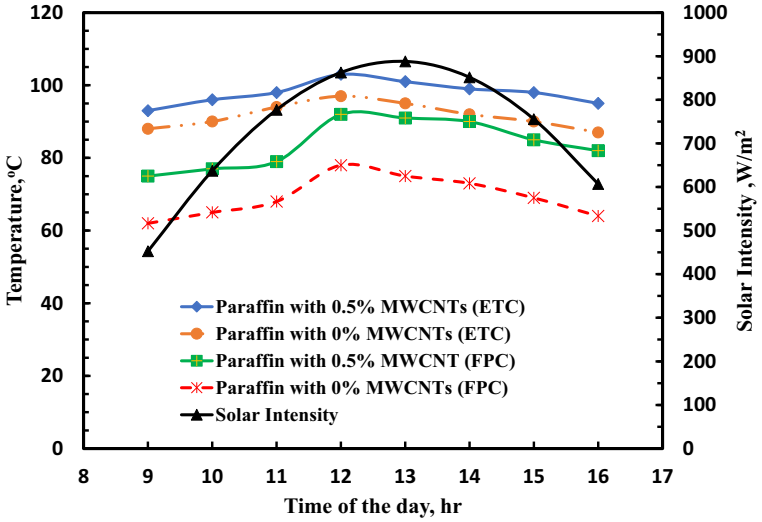

Figure 4. Distribution of solar radiation and collector's outlet temperature at different MWCNTs loadings with paraffin wax during the day.

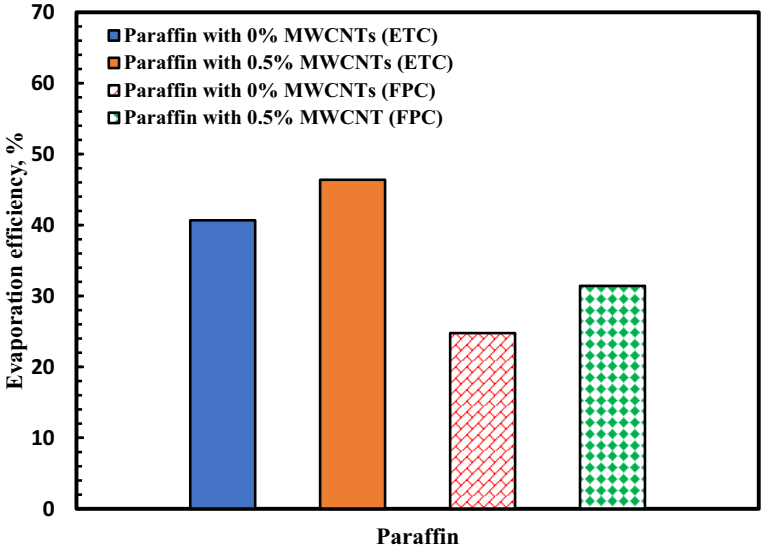

Figure 5. Comparison between the evaporation efficiency of solar collectors at different MWCNTs loadings with paraffin wax.

Fig. 6 shows the improvement in the amount of water evaporation through the FPC and ETC when 0.5 % MWCNTs loading is used with paraffin wax. This indicates that the evaporation rate was improved remarkably in the presence of MWCNTs in the base of paraffin wax. Since it is quite evident that by increasing the nanoparticles content from 0.0 to 0.5 %, the thermal conductivity of MWCNTs nanofluids increases. It is found that the amount of water evaporation rises from 2.6 to 3.3 kg d^{-1} for the FPC and from 4.27 to 4.87 kg d^{-1} for ETC.

Adding the nanoparticles to the fluid can improve the heat transfer efficiency by increasing the thermal conductivity such as microlayer evaporation and reformation of the thermal boundary layer. However, at high nanoparticle concentrations, a viscous nanofluid can lead to a slower internal fluid motion, which can be a limiting factor for evaporation at the free surface. Furthermore, the uneven surface can collect particles more easily and smooth the surface, resulting in a reduction in boiling performance.

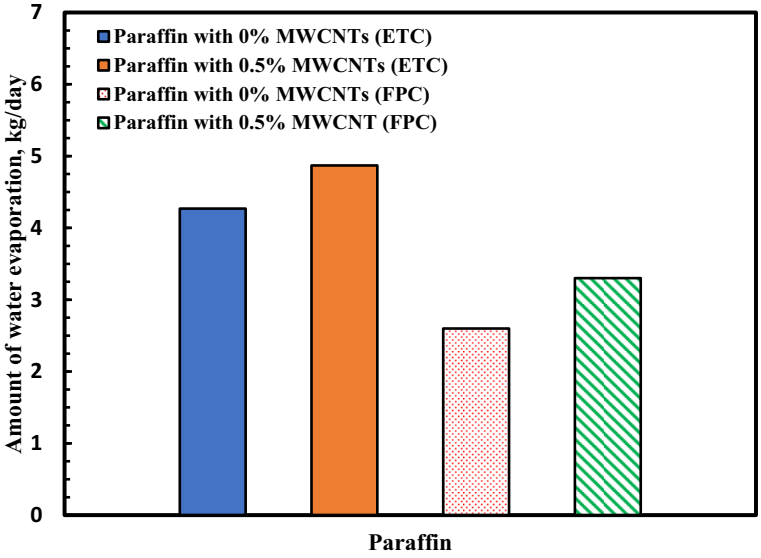

Figure 6. Comparison of the amount of water evaporation at different concentrations of MWCNTs with paraffin wax.

5.2 Using EG with FPC and ETC under Unsteady State Conditions

Fig. 7 demonstrates the experimental results of hourly variation of solar intensity with respect to operating time for four consecutive days from September 16 to 19, 2020. The figure shows a variation in solar intensity with time for the test day with a peak intensity of about 840 W m^{-2}. In addition, the result illustrates the distribution in measured outlet temperature from the FPC and ETC along the day. Temperature values were measured using 0.5 % MWCNTs loading in EG and pure fluid into a FPC with a seawater flow rate of 1.35 and 1.55 kg h^{-1}, respectively. All temperatures showed a similar behavior increase with rising solar radiation during the day.

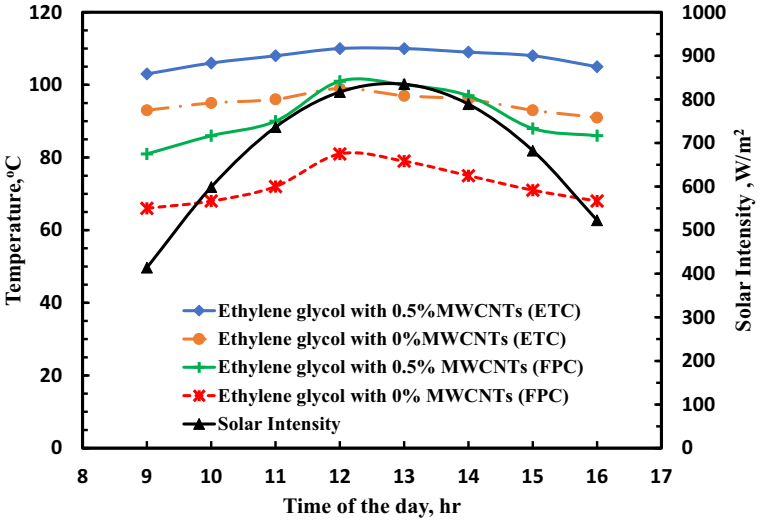

Figure 7. Distribution of solar radiation and collector outlet temperature at different MWCNTs loadings with ethylene glycol during the day.

Fig. 8 demonstrates the enhancement in the efficiency evaporation through the FPC and ETC when 0.5 % of MWCNTs loading is used with EG and compared to the case without MWCNTs. The evaporation efficiency of the FPC and ETC was clearly enhanced by using a higher MWCNTs loadings in the base EG, displaying improvements of about 36.3 and 33.67 %, respectively.

Fig. 9 illustrates the improvement in water evaporation through the FPC and ETC when 0.5 % of MWCNTs loading are mixed with EG and compared with pure EG at a seawater flow rate of 1.35 and 1.55 kg h^{-1}, respectively. It shows a significant enhancement in the rate of water evaporation in FPC and ETC systems using MWCNTs paraffin base. The amount of water evaporation increased up to 4.3 and 6.4 kg per day for the FPC and ETC, respectively.

In this system, the experiments were implemented using solar energy. Tabs. 6 and 7 summarize the results of FPC and ETC, respectively.

6 Conclusion

Nanofluids were applied to enhance the overall performance of solar thermal collectors in water desalination. It was found that increasing MWCNTs loadings (up to 0.5 wt %) leads to a higher evaporation rate. The nanofluids (paraffin wax + MWCNTs) showed significant improvement in distilled water productivity. In addition, the thermal energy storage of EG and paraffine wax was enhanced in the presence of MWCNTs.

The nanofluid (paraffin wax + MWCNTs 0.5 wt %) allowed for a substantial enhancement in distilled water productivity. In the ETC, the rate of water evaporation increased from 4.77 to 6.4 kg per day using the EG nanofluid. A remarkable

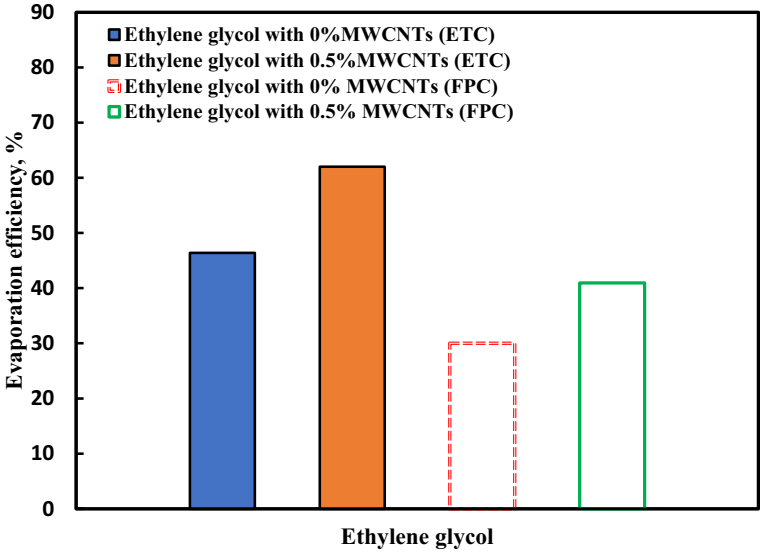

Figure 8. Comparison between the evaporation efficiency using ethylene glycol at different MWCNTs loadings.

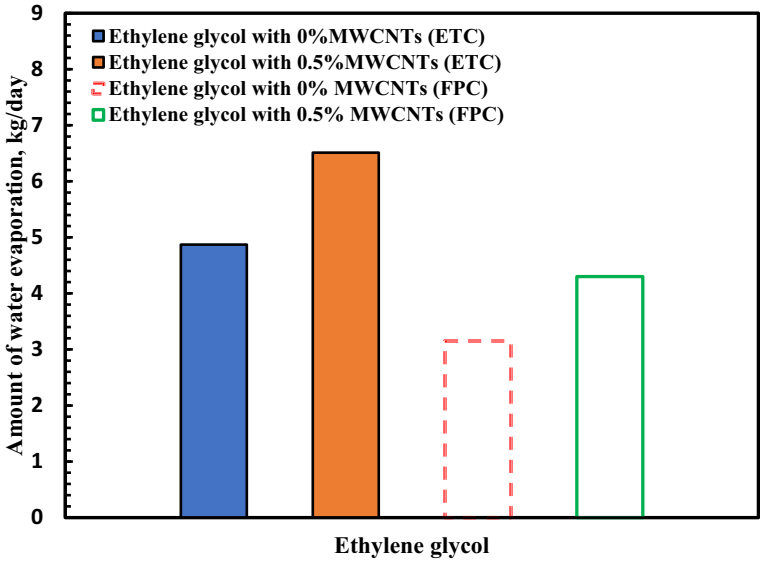

Figure 9. Comparison of the amount of water evaporation at different concentrations of MWCNTs with ethylene glycol.

Table 6. Summary of FPC results.

Material	Paraffin wax		Ethylene glycol	
FPC	0.0 % MWCNTs	0.5 % MWCNTs	0.0 % MWCNTs	0.5 % MWCNTs
Temperature range [°C]	62–78	75–92	66–81	81–100
Flow rate [kg h^{-1}]	1.35	1.35	1.35	1.35
Evaporation efficiency [%]	24.7	31.42	30	40.9
Amount of water evaporation [kg d^{-1}]	2.6	3.3	3.15	4.3
Improvement in efficiency [%]	–	27.5	–	36.3

increment in the rate of water evaporation was achieved in the presence of MWCNTs (0.5 wt %) with EG.

Acknowledgment

The authors would like to acknowledge the assistance provided by the Science and Technology Development Fund (STDF) for funding the project No. 41902 (Center of Excellence in Membrane-based Water Desalination Technology for Testing and Characterization).

The authors have declared no conflict of interest.

Symbols used

a	[–]	accuracy of device
A	[m^2]	area
C	[J $kg^{-1}K^{-1}$]	heat capacity
G	[W m^{-2}]	solar intensity
K	[W $m^{-1}K^{-1}$]	thermal conductivity
m	[kg s^{-1}]	mass flow rate
n	[–]	particle shape factor
Q_u	[W]	useful heat transfer
T_{ci}	[°C]	collector inlet temperature
T_{co}	[°C]	collector outlet temperature
u	[–]	standard uncertainty

Greek letters

η	[%]	thermal efficiency
ρ	[kg m^{-3}]	density
ϕ	[%]	volume concentration ratio of nanoparticles

Subscripts

bf	base fluid
c	collector
i	inlet

Table 7. ETC results.

Material	Paraffin wax		EG	
ETC	0.0 % MWCNTs	0.5 % MWCNTs	0.0 % MWCNTs	0.5 % MWCNTs
Temperature range [°C]	87–95	94–101	91–99	103–110
Flow rate [kg h^{-1}]	1.55	1.55	1.55	1.55
Evaporation efficiency [%]	40.66	46.38	46.38	62
Amount of water evaporation [kg d^{-1}]	4.71	5.32	4.77	6.4
Improvement in efficiency [%]	–	13	–	33.67

nf nanofluid
o outlet
p nanoparticle
v water evaporation
w seawater

Abbreviations

EG ethylene glycol
ETC evacuated-tube collector
FPC flat-plate collector
MWCNTs multiwalled carbon nanotubes

References

[1] I. Ali, O. A. Bamaga, L. Gzara, M. Bassyouni, M. H. Abdel-Aziz, M. F. Soliman, E. Drioli, M. Albeirutty, Assessment of blend PVDF membranes, and the effect of polymer concentration and blend composition, *Membranes* **2018**, *8 (1)*, 13.

[2] N. Rai, R. N. Hegde, Thermal performance enhancement of a helical coil-in-shell heat exchanger with circular finned turbulator and alumina nanofluid – An experimental study and correlation development, *J. Enhanced Heat Transfer* **2021**, *28 (1)*, 33–62.

[3] Z. Guo, A review on heat transfer enhancement with nanofluids, *J. Enhanced Heat Transfer* **2020**, *27 (1)*, 1–70.

[4] A. A. Alanezi, M. R. Safaei, M. Goodarzi, Y. Elhenawy, The effect of inclination angle and reynolds number on the performance of a direct contact membrane distillation (DCMD) process, *Energies* **2020**, *13 (11)*, 2824.

[5] N. A. S. Elminshawy, M. El-Ghandour, Y. Elhenawy, M. Bassyouni, D. G. El-Damhogi, M. F. Addas, Experimental investigation of a V-trough PV concentrator integrated with a buried water heat exchanger cooling system, *Sol. Energy* **2019**, *193*, 706–714.

[6] K. A. Alshibli, B. A. Alramahi, A. M. Attia, Assessment of spatial distribution of porosity in synthetic quartz cores using microfocus computed tomography (μCT), *Part. Sci. Technol.* **2006**, *24 (4)*, 369–380.

[7] S. Sagar, N. Iqbal, A. Maqsood, M. Shahid, N. A. Shah, T. Jamil, M. I. Bassyouni, Fabrication and thermal characteristics of functionalized carbon nanotubes impregnated polydimethylsiloxane nanocomposites, *J. Compos. Mater.* **2015**, *49 (8)*, 995–1006.

[8] A. A. I. Abd-Elmageed, A. F. Al-Hossainy, E. M. Fawzy, N. Almutlaq, M. R. Eid, A. Bourezgui, S. M. S. Abdel-Hamid, N. B. Elsharkawy, M. Zwawi, M. H. Abdel-Aziz, M. Bassyouni, Synthesis, characterization and DFT molecular modeling of doped poly (para-nitroaniline-co-para-toluidine) thin film for optoelectronic devices applications, *Opt. Mater.* **2020**, *99*, 109593.

[9] Y. Elhenawy, N. A. Elminshawy, M. Bassyouni, A. A. Alanezi, E. Drioli, Experimental and theoretical investigation of a new air gap membrane distillation module with a corrugated feed channel, *J. Membr. Sci.* **2020**, *594*, 117461.

[10] M. S. Zoromba, M. A. Tashkandi, A. A. Alshehri, M. H. Abdel-Aziz, M. Bassyouni, S. A. Mahmoud, A. B. Slimane, A. F. Al-Hossainy, Polymer solar cell based on doped o-anthranilic acid and o-aminophenol copolymer, *Opt. Mater.* **2020**, *104*, 109947.

[11] T. Yousefi, E. Shojaeizadeh, F. Veysi, S. Zinadini, An experimental investigation on the effect of pH variation of MWCNTs-H_2O nanofluid on the efficiency of flat-plate solar collectors, *Sol. Energy* **2012**, *86*, 771–779.

[12] W. Yu, H. Xie, D. Bao, Enhanced thermal conductivities of nanofluids containing graphene oxide nanosheets, *Nanotechnology* **2010**, *2*, 1–7.

[13] S. M. Peyghambarzadeh, S. H. Hashemabadi, M. Seifi Jamnani, S. M. Hoseini, Improving the cooling performance of automobile radiator with Al_2O_3/water Nanofluid, *Appl. Therm. Eng.* **2011**, *31 (10)*, 1833–1838.

[14] S. M. Peyghambarzadeh, S. H. Hashemabadi, S. M. Hoseini, M. Seifi Jamnani, Experimental study of heat transfer enhancement using water/ethylene glycol based nanofluids as a new coolant for car radiators, *Int. Commun. Heat Mass Transfer* **2011**, *38 (9)*, 1283–1290.

[15] M. Chandrasekar, S. Suresh, T. Senthilkumar, Mechanisms proposed through experimental investigations on thermophysical properties and forced convective heat transfer characteristics of various nano fluids, *Renewable Sustainable Energy Rev.* **2012**, *16 (6)*, 3917–3938.

[16] S. H. Hashemabadi, S. Etemad, Effect of rounded corners on the secondary flow of viscoelastic fluids through non-circular ducts, *Int. J. Heat Mass Transfer* **2014**, *49*, 1986–1990.

[17] R. A. Taylor, P. E. Phelan, T. P. Otanicar, C. A. Walker, M. Nguyen, S. Trimble, R. Prasher, Applicability of nanofluids in high flux solar collectors, *J. Renewable Sustainable Energy* **2011**, *3 (2)*, 23104.

[18] T. Yousefi, F. Veysi, E. Shojaeizadeh, S. Zinadini, An experimental investigation on the effect of Al_2O_3-H_2O nanofluid

on the efficiency of flat-plate solar collectors, *Renewable Energy* **2012**, *39 (1)*, 293–298.
[19] A. J. Moghadam, M. Farzane-Gord, M. Sajadi, M. Hoseyn-Zadeh, Effects of CuO/water nanofluid on the efficiency of a flat-plate solar collector, *Exp. Therm. Fluid Sci.* **2014**, *58*, 9–14.
[20] M. Karami, M. A. Akhavan Bahabadi, S. Delfani, A. Ghozatloo, A new application of carbon nanotubes nanofluid as working fluid of low-temperature direct absorption solar collector, *Sol. Energy Mater. Sol. Cells* **2014**, *121*, 114–118.
[21] Z. Said, M. Sabiha, R. Saidur, A. Hepbasli, N. Rahim, S. Mekhilef, T. Ward, Performance enhancement of a flat plate solar collector using titanium dioxide nanofluid and polyethylene glycol dispersant, *J. Cleaner Prod.* **2015**, *92*, 343–353.
[22] S. C. Lin, H. H. Al-Kayiem, Evaluation of copper nanoparticles – Paraffin wax compositions for solar thermal energy storage, *Sol. Energy* **2016**, *132*, 267–278.
[23] M. Assael, C. Chen, N. Metaxa, W. Wakeham, Thermal conductivity of suspensions of carbon nanotubes in water, *Int. J. Thermophys.* **2004**, *25*, 971–985.
[24] W. Yu, H. Xie, L. Chen, Y. Li, Investigation of thermal conductivity and viscosity of ethylene glycol based ZnO nanofluid, *Thermochim. Acta* **2009**, *491*, 92–96.
[25] M. C. Daniel, D. Astruc, Gold nanoparticles: Assembly, supramolecular chemistry, quantum-size-related properties, and applications toward biology, catalysis, and nanotechnology, *Chem. Rev.* **2004**, *104*, 293–346.
[26] C. W. Corti, R. J. Holliday, D. T. Thompson, Developing new industrial applications for gold: Gold nanotechnology, *Gold Bull.* **2002**, *35*, 111–117.
[27] A. Elminshawy, K. Morad, N. A. Elminshawy, Y. Elhenawy, Performance enhancement of concentrator photovoltaic systems using nanofluids, *Int. J. Energy Res.* **2021**, *45 (2)*, 2959–2979.
[28] S. M. S. Abdel-Hamid, O. A. Al-Qabandi, N. A. S. Elminshawy, M. Bassyouni, M. S. Zoromba, M. H. Abdel-Aziz, H. Mira, Y. Elhenawy, Fabrication and characterization of microcellular polyurethane sisal biocomposites, *Molecules* **2019**, *24 (24)*, 4585.
[29] B. Ul Islam, A. Mukhtar, S. Saqib, A. Mahmood, S. Rafiq, A. Hameed, M. Ibrahim, Thermal conductivity of multi-walled carbon nanotubes-kapok seed oil-based nanofluid, *Chem. Eng. Technol.* **2020**, *43 (8)*, 1638–1647.
[30] M. Bassyouni, A. E. Mansi, A. Elgabry, B. A. Ibrahim, O. A. Kassem, R. Alhebeshy, Utilization of carbon nanotubes in removal of heavy metals from wastewater: A review of the CNTs' potential and current challenges, *Appl. Phys. A* **2020**, *126 (1)*, 1–33.
[31] Y. Elhenawy, G. Hafez, S. Abdel-Hamid, M. Elbany, Prediction and assessment of automated lifting system performance for multi-storey parking lots powered by solar energy, *J. Cleaner Prod.* **2020**, *266*, 121859.
[32] M. S. Zoromba, S. Alghool, S. M. S. Abdel-Hamid, M. Bassyouni, M. H. Abdel-Aziz, Polymerization of aniline derivatives by $K_2Cr_2O_7$ and production of Cr_2O_3 nanoparticles, *Polym. Adv. Technol.* **2017**, *28 (7)*, 842–848.
[33] V. Selvaraj, K. Senthilkumar, H. Krishnan, Covalent functionalization of graphene for the enhancement of thermophysical properties in nanofluids, *Chem. Eng. Technol.* **2021**, *44 (5)*, 811–818.
[34] H. Yarmand, S. Gharehkhani, S. F. S. Shirazi, A. Amiri, E. Montazer, H. K. Hamed Khajeh Arzani, R. Sadri, M. Mahidzal Dahari, S. N. Kazi, Nanofluid based on activated hybrid of biomass carbon/graphene oxide: Synthesis, thermophysical and electrical properties, *Int. Commun. Heat Mass Transfer* **2016**, *72*, 10–15.
[35] J. A. Eastman, U. S. Choi, S. Li, L. J. Thompson, S. Lee, Enhanced thermal conductivity through the development of nanofluids, in *Proc. of the Materials Research Soc. Symp.*, Vol. 457, Materials Research Society, Pittsburgh, PA **1997**, 3–11.
[36] M. Karami, M. A. A. Bahabadi, S. Delfani, A. Ghozatloo, A new application of carbon nanotubes nanofluid as working fluid of low-temperature direct absorption solar collector, *Sol. Energy Mater. Sol. Cells* **2014**, *121*, 114–118.
[37] F. Marquis, L. Chibante, Improving the heat transfer of nanofluids and nanolubricants with carbon nanotubes, *JOM* **2005**, *57*, 32–43.
[38] S. U. S. Choi, Z. G. Zhang, W. Yu, F. E. Lockwood, E. A. Grulke, Anomalous thermal conductivity enhancement in nanotube suspensions, *Appl. Phys. Lett.* **2001**, *79*, 2252–2254.
[39] A. Indhuja, K. S. Suganthi, S. Manikandan, K. S. Rajan, Viscosity and thermal conductivity of dispersions of gum arabic capped MWCNT in water: Influence of MWCNT concentration and temperature, *J. Taiwan Inst. Chem. Eng.* **2013**, *44*, 474–479.
[40] Z. Y. Luo, C. Wang, W. Wei, G. Xiao, M. J. Ni, Performance improvement of a nanofluid solar collector based on direct absorption collection (DAC) concepts, *Int. J. Heat Mass Transfer* **2014**, *75*, 262–271.
[41] N. A. S. Elminshawy, M. A. Gadalla, M. Bassyouni, K. El-Nahhas, A. Elminshawy, Y. Elhenawy, A novel concentrated photovoltaic-driven membrane distillation hybrid system for the simultaneous production of electricity and potable water, *Renewable Energy* **2020**, *162*, 802–817.
[42] S. M. S. Hosseini, M. S. Dehaj, Assessment of TiO_2 water-based nanofluids with two distinct morphologies in a U type evacuated tube solar collector, *Appl. Therm. Eng.* **2021**, *182*, 116086.
[43] D. Das, U. Bordoloi, P. Kalita, R. F. Boehm, A. D. Kamble, Solar still distillate enhancement techniques and recent developments, *Groundwater Sustainable Dev.* **2020**, *10*, 100360.
[44] D. Huang, Z. Wu, B. Sunden, Pressure drop and convective heat transfer of Al_2O_3/water and MWCNT/water nanofluids in a chevron plate heat exchanger, *Int. J. Heat Mass Transfer* **2015**, *89*, 620–626.
[45] T. Boldoo, J. Ham, H. Cho, Comparison study on photothermal energy conversion performance of functionalized and non-functionalized MWCNT nanofluid, *Energies* **2019**, *12 (19)*, 3763.
[46] N. Ukrainczyk, S. Kurajica, J. Šipušić, Thermophysical comparison of five commercial paraffin waxes as latent heat storage materials, *Chem. Biochem. Eng. Q.* **2010**, *24 (2)*, 129–137.
[47] Å. Melinder, Properties and other aspects of aqueous solutions used for single phase and ice slurry applications, *Int. J. Refrig.* **2010**, *33 (8)*, 1506–1512.

[48] Y. Xuan, W. Roetzel, Conceptions for heat transfer correlation of nanofluids, *Int. J. Heat Mass Transfer* **2000**, *43 (19)*, 3701–3707.
[49] P. Van Trinh, N. N. Anh, B. H. Thang, N. T. Hong, N. M. Hong, P. H. Khoi, P. N. Hong, Enhanced thermal conductivity of nanofluid-based ethylene glycol containing Cu nanoparticles decorated on a Gr-MWCNT hybrid material, *RSC Adv.* **2017**, *7 (1)*, 318–326.
[50] S. Elhady, M. Bassyouni, R. A. Mansour, M. H. Elzahar, S. Abdel-Hamid, Y. Elhenawy, M. Y. Saleh, Oily wastewater treatment using polyamide thin film composite membrane technology, *Membranes* **2020**, *10 (5)*, 84.
[51] A. M. Sandid, M. Bassyouni, D. Nehari, Y. Elhenawy, Experimental and simulation study of multichannel air gap membrane distillation process with two types of solar collectors, *Energy Convers. Manage.* **2021**, *243*, 114431.
[52] H. A. Maddah, M. Bassyouni, M. H. Abdel-Aziz, M. S. Zoromba, A. F. Al-Hossainy, Performance estimation of a mini-passive solar still via machine learning, *Renewable Energy* **2020**, *162*, 489–503.
[53] A. A. Alanezi, M. Bassyouni, S. Abdel-Hamid, H. S. Ahmed, M. H. Abdel-Aziz, M. S. Zoromba, Y. Elhenawy, Theoretical investigation of vapor transport mechanism using tubular membrane distillation module, *Membranes* **2021**, *11 (8)*, 560.

